Journal of Hydrology 633 (2024) 130957

Contents lists available at ScienceDirect

Journal of Hydrology

journal homepage: www.elsevier.com/locate/jhydrol

Potential of ground-penetrating radar to calibrate electromagnetic induction for shallow soil water content estimation

Sashini Pathirana [a,*], Sébastien Lambot [b], Manokararajah Krishnapillai [a], Christina Smeaton [a], Mumtaz Cheema [a], Lakshman Galagedara [a]

[a] School of Science and the Environment, Memorial University of Newfoundland, Corner Brook, Newfoundland, Canada
[b] Earth and Life Institute, Université catholique de Louvain, 1348 Louvain-la-Neuve, Belgium

ARTICLE INFO

This manuscript was handled by Carla Saltalippi, Editor-in-Chief, with the assistance of Corrado Corradini, Associate Editor

Keywords:
Apparent electrical conductivity
Electromagnetic induction
Ground-penetrating radar
Sampling volume
Soil water content
Prediction model

ABSTRACT

Ground-penetrating radar (GPR) and electromagnetic induction (EMI) are used to determine and map soil water content (SWC) in the agricultural landscape. While GPR provides a straightforward estimation of SWC, EMI requires site-specific calibrations mainly based on point-scale measurements such as time domain reflectometry (TDR). However, there is a significant difference in the measurement volumes between EMI and point-scale TDR measurements. This study aimed to enhance the calibration of EMI for estimating SWC in the agricultural landscape by leveraging the larger sampling volumes provided by GPR. Apparent electrical conductivity (EC_a) from a multi-coil EMI sensor and dielectric constant from GPR with two center frequencies (500 MHz and 250 MHz) were collected as soil proxies along with TDR measurements. Calibration models were developed under irrigated conditions and the model evaluation was conducted under natural moisture conditions. Correlations were assessed between the proxies from GPR and EMI with TDR-derived SWCs. Simple linear regression (SLR) models were developed between EMI and GPR data to predict SWC. Strong positive correlations ($r \geq 0.80$) were observed between the proxies (GPR and the shorter inter-coil spacing (0.32 m) of EMI) and TDR-measured SWC. EC_a data from vertical and horizontal coil orientations of the shorter inter-coil spacings were selected to develop SLR models with GPR. The SLR models with the GPR 500 MHz frequency showed a higher coefficient of determination ($R^2 > 0.70$) for both coil orientations of EMI. Results showed the potential of using GPR to calibrate EMI for shallow SWC estimation (below 0.5 m). Nevertheless, the EMI estimated SWCs were not effectively verified with GPR-estimated SWCs, which could be attributed to specific site conditions in the study area. Further research must focus on improving the calibration and model evaluation by incorporating the variability of other soil parameters (soil porosity, pore-water conductivity, and soil salinity) that may affect the SWC–EC_a relationship.

1. Introduction

The variability of soil water content (SWC) is significant both in space and time, and it plays a crucial role in maintaining healthy soil ecosystems. Real-time monitoring of SWC is vital for agriculture as it controls water balance in the vadose zone, plant growth and crop yield, nutrient absorption, and soil health (Vereecken et al., 2008, 2016; Wijewardana and Galagedara, 2010). Furthermore, SWC controls physical (e.g., penetration resistance, soil temperature, and saturation), chemical (e.g., soil salinity, nitrogen mineralization, soil pH), and biological (e.g., microbial activity) soil properties, states and processes that affect plant growth (Robinson et al., 2008). In precision agriculture, spatial and temporal variability of SWC is crucial to managing resources for optimizing crop yields with minimum inputs and scheduling irrigation.

SWC estimation ranges from large scales over several kilometers using remote sensing approaches (e.g., satellite, drones and airborne remote sensing) to small-scale point measurements (e.g., soil sampling and sensors like Time Domain Reflectometry (TDR)) covering a few centimeters (Robinson et al., 2008; Turkeltaub et al., 2022; Vereecken et al., 2014). Ground-penetrating radar (GPR) and electromagnetic induction (EMI) are near-surface geophysical techniques that utilize

* Corresponding author.
E-mail addresses: epspathirana@mun.ca (S. Pathirana), sebastien.lambot@uclouvain.be (S. Lambot), n62mk@mun.ca (M. Krishnapillai), csmeaton@mun.ca (C. Smeaton), macheema@mun.ca (M. Cheema), lgalagedara@mun.ca (L. Galagedara).

https://doi.org/10.1016/j.jhydrol.2024.130957
Received 19 July 2023; Received in revised form 3 February 2024; Accepted 13 February 2024
Available online 28 February 2024

electromagnetic fields. These methods can be used to assess and map the spatial and temporal variability of SWC. These two techniques fall between remote sensing and point-scale measurements (Binley et al., 2015; Doolittle and Brevik, 2014; Huisman et al., 2003; Klotzsche et al., 2018). Moreover, GPR and EMI are non-destructive, labour and time-saving, and cost-effective SWC estimation methods, thereby offering additional benefits over standard methods (Doolittle and Brevik, 2014; Liu et al., 2019; Pathirana et al., 2023). Furthermore, GPR and EMI provide higher-resolution information with a more extensive spatial coverage with geo-referenced data to estimate and map the SWC in the agricultural landscape (Klotzsche et al., 2018; Robinson et al., 2008; Rubin and Hubbard, 2005; Toy et al., 2010).

GPR uses high-frequency electromagnetic waves (usually in the range of 10–3600 MHz), while EMI uses relatively low-frequency ranges (usually in the range of 1–100 kHz) (Davis and Annan, 1989; Klotzsche et al., 2018). EMI and GPR responses are primarily related to subsurface electrical parameters whereby mainly the dielectric constant (K_r) and apparent electrical conductivity (EC_a) are the proxies measured by GPR and EMI, respectively (Annan, 2005; Doolittle and Brevik, 2014). GPR-based SWC estimation has been widely used in agricultural research. The K_r values varies from 1 (air) to 80 (water), with all other materials falling within this range. Therefore, the K_r of soil is mainly controlled by the SWC (Davis and Annan, 1989; Topp et al., 1980). SWC influences the propagation wave velocity of GPR since the velocity varies with K_r (Annan, 2005). In GPR applications, the Topp equation is often used to estimate SWC from K_r (Topp et al., 1980). Direct ground wave velocity (V_{DGW}), reflected wave velocity, transmitted wave velocity and reflection amplitudes are used to assess volumetric SWC with GPR. Previous studies estimated and mapped the spatial and temporal variability of shallow SWC (<50 cm) with GPR V_{DGW} and validated successfully with standard methods such as TDR and thermo-gravimetric methods (Chanzy et al., 1996; Galagedara et al., 2003a; Grote et al., 2010; Huisman et al., 2001; Mahmoudzadeh Ardekani, 2013). Advanced full-wave modelling and radar data inversion enable automated and real-time soil moisture mapping (Minet et al., 2012; Wu et al., 2019, 2022). While EMI measures the EC_a of the subsurface soil, which is a weighted average value of the bulk soil EC of the solid and solution conductivities over a specific sensing depth range. The sensing depth and sampling volume are dependent on the coil orientations, vertical coplanar (VCP) and horizontal coplanar (HCP), and inter-coil spacings of the transmitter and the receiver (McNeill, 1980). SWC strongly influences EC_a, therefore, empirical regression models are often developed between EC_a measured by EMI and SWC (Altdorff et al., 2017; Badewa et al., 2018; Brevik et al., 2006; Kachanoski et al., 1988; Martini et al., 2017a; Robinet et al., 2018). The majority of studies show site-specific linear empirical relationships between the SWC and EC_a (Brevik et al., 2006; Calamita et al., 2015; Robinson et al., 2012; Turkeltaub et al., 2022; Mensah et al., 2023a, 2023b), with fewer showing non-linear relationships (Kachanoski et al., 1988; Robinet et al., 2018). Besides SWC, soil EC_a depends on other parameters, including soil texture, temperature, bulk density/porosity, pore-water electrical conductivity and mineralogy (Altdorff et al., 2017; Friedman, 2005; Martini et al., 2017b; Robinet et al., 2018). Therefore, SWC predictions with EC_a are complex and require site-specific calibrations (Altdorff et al., 2017; Turkeltaub et al., 2022).

TDR has been commonly used as a standard method to compare GPR and EMI estimated SWC during the past two decades. Similar to GPR, TDR is used to estimate SWC based on K_r and provides a point-scale measurement over the length and spacing between the rods of the probe since it uses guided waves (Jones et al., 2002; Weiler et al., 1998). Moreover, TDR covers a relatively smaller sampling volume than the depth and the footprint of GPR and EMI depending on the system configuration and sensor geometry (Evett and Parkin, 2005; Ferré et al., 1996). In addition, TDR probes must be inserted or installed. It creates small-scale disturbance affecting microscale water flow patterns and installing TDR probes is difficult in most field conditions/applications, specifically beyond the 0.20 m depth range. Nevertheless, TDR probes are usually installed in the soil, providing the capability to capture the SWC variability with various resolutions across different time laps. This feature is highly valuable for investigating the temporal fluctuations in SWC in the agricultural landscape.

The sampling volume of EMI and point-scale TDR measurements are different (Fig. 1). Thus, spatial scale heterogeneity of measured SWC varies between the two methods. For example, a relatively large sample volume of EMI gives an average SWC over the footprint and sampling depth. In contrast, TDR captures the small-scale heterogeneity of SWC (Fig. 1). In this respect, many sampling locations and depths are needed with these point-scale measurements to represent the spatial coverage of EMI (sampling depth and footprint) and for developing and evaluating accurate site-specific prediction models. This ground-truthing process is often tedious, time-consuming, and destructive. On the other hand, GPR has the advantage of directly relating the radar wave (either direct or reflected wave) velocity to SWC changes without using empirical relationships/site-specific calibrations like EMI (Steelman and Endres, 2011). Toy et al. (2010) examined the temporal variation of SWC with EC_a and V_{DGW} in three texturally different study sites. They compared EMI and GPR and found that EC_a ($R^2 < 0.75$) and V_{DGW} ($R^2 < 0.90$) correlated well with the thermo-gravimetric method at the silt loam site compared to the sand and sandy loam sites (Toy et al., 2010). Generally, the lower accuracy of the EC_a-SWC relationship in coarse-textured soils compared to fine-textured soils could potentially explain this observation.

Compared to the point-scale measurements, both EMI and GPR can cover multiple depths without any disturbances. Multi-coil and multi-frequency EMI sensors with VCP and HCP coil orientations can cover different sampling depths (McNeill, 1980). As for GPR, sampling depth increases with decreasing the operating frequency (Annan, 2005). However, EMI can sense different depths simultaneously compared to the GPR when using multi-coil or multi-frequency sensors. In addition, EMI can also provide key soil information other than SWC, such as soil salinity, porosity, and clay content, which are essential for decision-making in precision agriculture. Additionally, when conducting surveys on agricultural lands with crops, on-ground GPR encounters contact issues known as ground-coupling. This problem is absent in off-ground GPR and EMI techniques, as these instruments are positioned at a distance above the ground. However, it is important to note that off-ground GPR primarily captures surface reflections in agricultural fields, typically sensitive to the top 50 cm of soil depth, depending on the frequency range (Wu and Lambot, 2022).

Considering these factors, we hypothesize that GPR can be used to calibrate EMI for accurate estimation of SWC. Therefore, the calibration model would cover a larger sampling volume than the point-scale measurements. This novel approach facilitates the development of SWC prediction models to estimate and map spatial (vertical and horizontal scales) and temporal variability of SWC non-destructively. This study aimed to develop and evaluate calibration models for EMI to estimate SWC using GPR as ground truth. Accordingly, the specific objectives of this study were to: (1) correlate two proxies; K_r from on-ground GPR and EC_a from EMI, with SWC measured from TDR (SWC_{TDR}); (2) assess the accuracy of GPR estimated SWC (SWC_{GPR}) in order to calibrate and evaluate EMI; and (3) develop and evaluate calibration models for EMI to estimate SWC, using GPR. This study developed site-specific predictive regression models between SWC_{GPR} and EMI measurements to predict SWC. Hereafter these predictive regression models will be referred to as “calibration”.

2. Methodology

2.1. Study area

The study was conducted at the Western Agriculture Center and Research Station, Pynn's Brook, Pasadena, (49°04′20″N, 57°33′35″W),

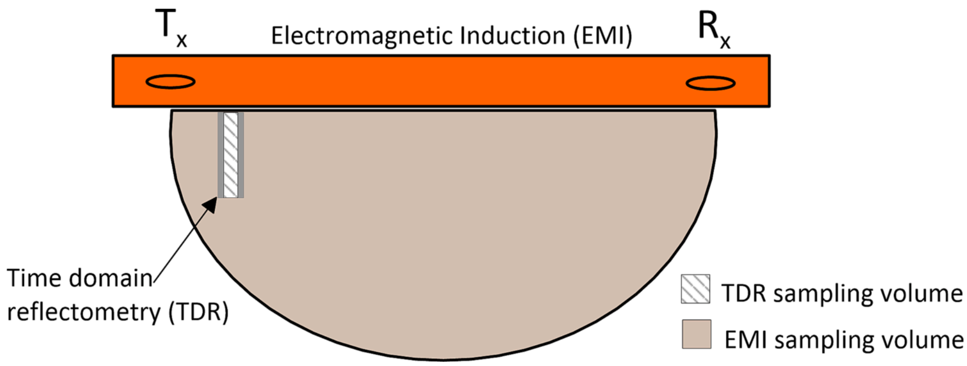

Fig. 1. Representation of the different sampling volumes of electromagnetic induction (EMI) and time domain reflectometry (TDR).

Newfoundland, Canada (Fig. 2), which is managed by the Department of Fisheries, Forestry and Agriculture, Government of Newfoundland and Labrador, Canada. The site is a fallow grassland with no agricultural activity during the past eight years. The soil texture in the 0–0.50 m depth of the site is loamy sand (sand = 83.0 % (±1.25); silt = 14.6 % (±1.21); clay = 2.4 % (±0.04); $n = 25$), soil organic matter content (dry mass basis) is 4.18 % (±0.39; $n = 25$), and the average bulk density is 1.31 (±0.01; $n = 25$) g/cm^3. According to the Canadian soil classification, the loamy sand soil at the studied site is characterized as an orthic humic podzol (Soil Classification Working Group, 1998).

2.2. Field data collection

Two different data acquisition approaches were implemented at the study site: (1) calibration of EMI using the on-ground GPR method under background and irrigated conditions; and (2) evaluation of the calibration models under natural moisture conditions. A 3 m × 6 m area was selected for the calibration, and a 9 m × 6 m (*i.e.*, three times larger) area was selected for the evaluation.

Under the irrigation, 20 mm of fresh water (EC = 1 mS/m) was applied uniformly using a shower head to the calibration study area/plot. The irrigated water amount was calculated to increase the SWC by 10 % from the background SWC, based on 0.20 m soil depth. From 0 to 0.20 m depth was considered since it is a dynamic interface between the soil, vegetation, atmosphere, and human activities, impacted by precipitation, evaporation, and infiltration. Additionally, this research focused on estimating SWC at the shallow root zone to support precision agriculture. GPR and EMI surveys and TDR data collections were conducted in two stages in the calibration data set: (1) before irrigation as background (BKG); and (2) after the end of irrigation (EOI). Model evaluation data were collected in an adjacent area next to the calibrated area (including the calibrated area) to examine the applicability of the regression models developed during the calibration under the natural SWC variability. System configuration and survey set-up for EMI and GPR data acquisition were the same in calibration and model evaluation data sets.

EMI surveys were conducted in continuous mode, using a multi-coil EMI sensor (CMD-MINIEXPLORER, GF instruments, Czech Republic) with an EMI frequency of 30 kHz. The instrument has one transmitter coil and three receiver coils in three different inter-coil spacings (offset 1 = 0.32 m, offset 2 = 0.71 m, and offset 3 = 1.18 m). Two separate surveys were carried out for VCP and HCP coil orientations. These inter-coil spacings and coil orientations resulted in six integrated depths of measured EC_a data (see Appendix Fig. A.1). The depth range covered by coil 2 and 3 is beyond the scope of the sampling depth of this study. Therefore, coils 2 and 3 were excluded from further analysis. The instrument was factory calibrated. Prior to each survey, the instrument was warmed up for a minimum of 30 min. Given the CMD's high temperature stability (Guide for electromagnetic conductivity mapping and tomography – GF instruments), no instrumental drift in EC_a measurements was anticipated. During the surveys, the instrument was consistently carried out using a handle with an average height of 0.20 m above the ground, and the same person conducted all the surveys to maintain a constant height and speed. EMI surveys were conducted at 0.5 m intervals starting from the 0 m line in the X direction resulting in 7 survey lines for the calibration data set (Fig. 3a) and 19 survey lines for the evaluation data set (Fig. 3b).

GPR data were collected by employing 500 MHz and 250 MHz center frequency GPR transducers (PulseEKKOPro, Sensors and Software, Canada) with the settings in Table 1. GPR survey lines were carried out in fixed offset method survey mode at 1 m line intervals starting from the 0.5 m line in the X direction resulting in three survey lines for the calibration data set (Fig. 3a) and nine survey lines for the model evaluation data set (Fig. 3b). A field-calibrated TDR sensor with 0–0.20 m probe length was used to measure SWC, and measurements were taken at five selected locations in each sub-plot in the calibration data set. Three measurements were taken at each data collection location to get an average TDR value for each location to roughly cover the GPR and

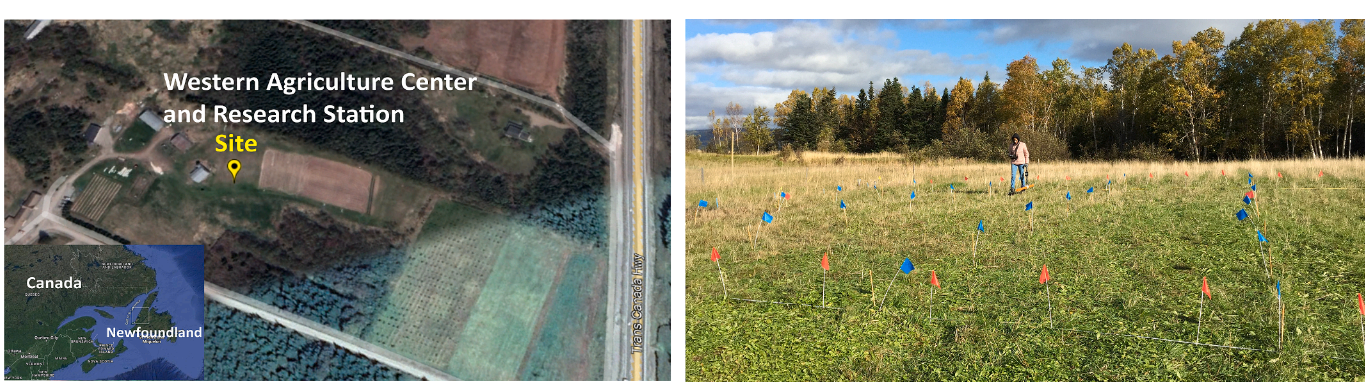

Fig. 2. The study site located at the Western Agriculture Center and Research Station, Pasadena, Newfoundland, Canada (49°04′20″N, 57°33′35″W).

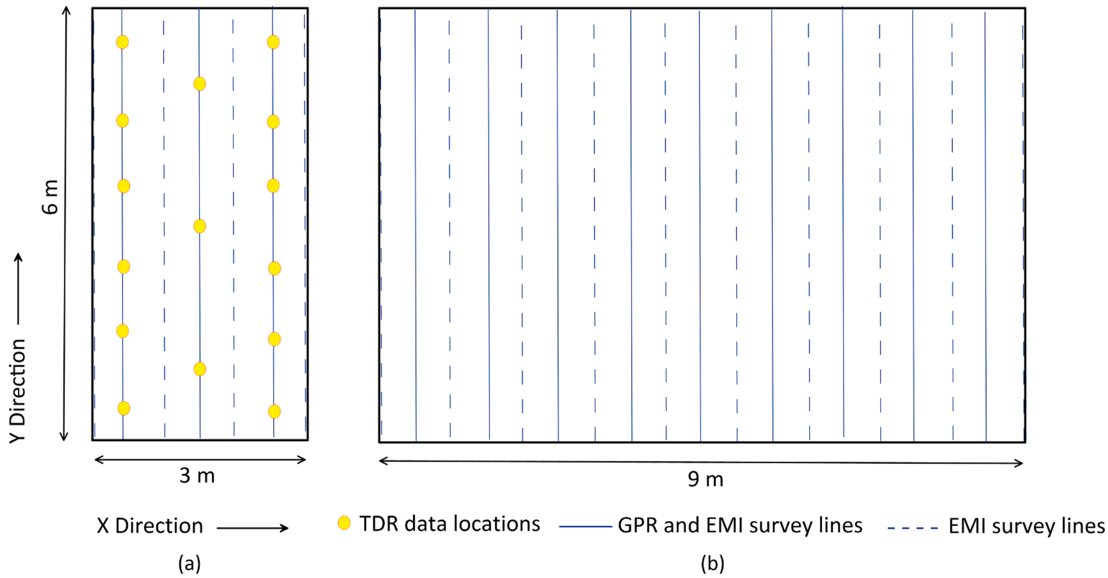

Fig. 3. Field diagram showing the data collection procedure and plots for calibration and evaluation: (a) calibration of electromagnetic induction (EMI) using ground-penetrating radar (GPR) under background (BKG) and irrigated (EOI) conditions, and (b) evaluation of the calibration models under natural moisture conditions.

Table 1
Ground-penetrating radar (GPR) settings under two center frequencies.

Settings	250 MHz	500 MHz
Antenna separation	0.38 m	0.23 m
Antenna step-size	0.05 m	0.05 m
Time window	100 ns	50 ns
Sampling interval	0.4 ns	0.2 ns
Stacking	32	32
Gain	Auto-gain	Auto-gain

EMI footprint (Fig. 3a).

2.3. Data processing

The subsurface electrical properties are affected by soil temperature, which is not stable; therefore, the measured EC_a values with EMI were first corrected for temperature differences in different stages (BKG – 20.6 °C (±0.1) and EOI – 28.5 °C (±0.2)) in the calibration data set and evaluation data set (20.5 °C (±0.1)). EC_a is expressed at the reference temperature of 25 °C. By using Eqs. (1) and (2), EC_a measured at an actual temperature t (EC_t) can be converted to the EC_a at 25 °C (EC_{25}) (Corwin and Lesch, 2005; Sheets and Hendrickx, 1995), where f_t is the temperature conversion factor.

$$f_t = 0.4470 + 1.4034e^{-t/26.815} \quad (1)$$

$$EC_{25} = f_t \cdot EC_t \quad (2)$$

GPR data were corrected for the time zero shift and processed by applying bandpass and dewow filters and gain functions. The direct ground wave travel times were picked using the GPR processing software's assisted pick processing tool and converted to velocities (V_{DGW}). Then, respective K_r was calculated using Eq. (3), where c is the speed of electromagnetic waves in the free space, *i.e.,* 0.3 m/ns (Annan, 2005). Volumetric SWC was calculated using the petrophysical relationship proposed by Topp et al. (1980) Eq. (4).

$$K_r = \left(\frac{c}{V_{DGW}}\right)^2 \quad (3)$$

$$SWC = -5.3 \times 10^{-2} + 2.92 \times 10^{-2}K_r - 5.5 \times 10^{-4}K_r^2 + 4.3 \times 10^{-6}K_r^3 \quad (4)$$

Variograms were fitted for the temperature-corrected EC_a data and GPR-estimated SWC data. Variogram fitting parameters and ordinary (point) kriging were used to prepare the interpolated EC_a and SWC maps. Data points were digitized for selected locations to obtain EC_a and SWC data for statistical analysis. For the calibration data set, 15 locations were selected for digitizing based on the TDR data locations. For the evaluation data set, 270 data points were digitized in 0.2 m intervals (30 data points per line) along the Y directions in all the 9 GPR survey lines (Fig. 3).

Sampling depths (D) were calculated for different GPR frequencies using Eq. (5) proposed by Galagedara et al. (2005). This equation was initially developed for a sandy loam soil under wet and dry conditions. Subsequently, it was found to be equally effective when applied to sandy soils (Grote et al., 2010). The equation was selected since the studied site predominantly contains more than 80 % of sand. In Eq. (5), λ is the wavelength, calculated using the operation frequency and propagation wave velocity.

$$D = 0.6015\lambda + 0.0468 \quad (5)$$

2.4. Statistical analysis

One-way analysis of variance (one-way ANOVA) tests were carried out for the calibration data set to see the treatment effect (irrigation) on the proxies from EMI (EC_a) and GPR (K_r) with SWC_{TDR}. The null hypothesis was that the group means of BKG and EOI were equal at the 0.05 significance level.

Correlation analyses were carried out between SWC_{TDR} and proxies from GPR (K_r estimated from 500 MHz (K_{r500}) and 250 MHz (K_{r250})) and EMI (EC_a from coil 1 vertical coplanar (VCP_1), and horizontal coplanar (HCP_1)) collected during the BKG and EOI stages in the calibration data set (Fig. 4). Principle component analysis (PCA) was done to select significant variables before carrying out regression models. For the PCA, SWC_{TDR}, and SWC estimated from GPR 500 MHz (SWC_{500}) and 250 MHz (SWC_{250}), and coil 1 EC_a data of two coil orientations (VCP_1 and HCP_1) from EMI were plotted. Based on the PCA results, the best correlated coil orientations of EMI and GPR frequencies were selected for further analysis (Fig. 4).

In this study, GPR-estimated SWC was used to calibrate the EMI instrument by correlating SWC_{GPR} with EC_a data. Therefore, two GPR-estimated SWCs (SWC_{500} and SWC_{250}) were compared with SWC_{TDR}

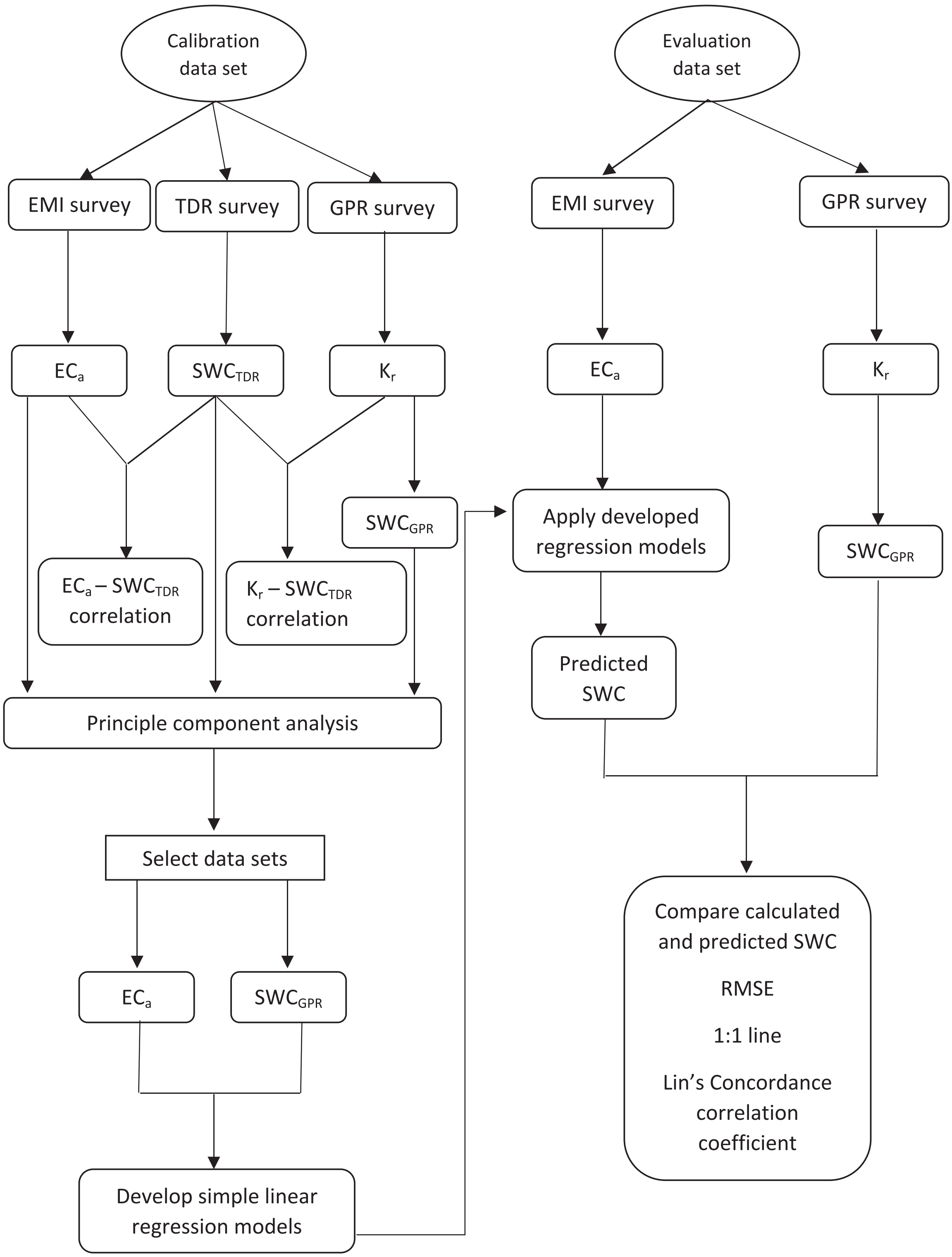

Fig. 4. Flow chart of the statistical data analysis for model calibration and evaluation.

using the 1:1 line.

Regression models were developed with the selected EC_a data sets and GPR frequencies based on the results of the one-way ANOVA, correlation analysis, and PCA. The novel approach used in this study was to calibrate EC_a (EMI measured) with GPR, as both methods have a sampling volume somewhat similar when compared to point-scale SWCs measured with TDR. Therefore, SWC_{TDR} was not used to develop regression models for EC_a. The developed regression models were then applied to another set of SWC_{GPR} under natural moisture conditions (model evaluation data set) to assess the prediction accuracy. GPR-estimated, and EMI-predicted SWCs were tested statistically using the 1:1 line, RMSE, and Lin's concordance correlation coefficient (Fig. 4). All the statistical analyses were done at the 5 % probability level ($\alpha = 0.05$).

3. Results and discussion

3.1. Analysis of variance and variability of data

The null hypothesis assumed that the mean values in both stages, BKG and EOI, were equal. According to the results of the one-way ANOVA, the probability value (p-value) is lower than the 0.05 significant level (Table 2). Consequently, the null hypothesis is rejected, signifying that not all means are equal. F values explain the variation between the group and within the group. F-value is higher than the $F_{critical}$ value (4.196) in the data set (Table 2). Therefore, the mean difference is significant in the data set at the 0.05 significance level. The letters (a, b) indicate significant differences within each stage of BKG and EOI based on the Tukey's tests (Table 2). With the applied irrigation, SWC increased from BKG to EOI; therefore, SWC_{TDR}, K_{r500}, and K_{r250} increased as expected. On the other hand, when increasing SWC, EC_a also increases (Calamita et al., 2015; Toy et al., 2010). VCP_1 and HCP_1 showed an increasing trend in EC_a with applied irrigation. Accordingly, one-way ANOVA showed that SWC_{TDR}, K_{r500}, K_{r250}, VCP_1, and HCP_1 data significantly differed from BKG to EOI in the calibration data set.

3.2. Correlation between soil water content and proxies

Correlations between SWC_{TDR} and proxies from GPR and EMI showed different strengths and directions for the calibration data set in the 0.05 significance level. K_{r500} and K_{r250} showed strong positive correlations with SWC_{TDR}, as expected. K_{r500} showed a higher correlation (*r = 0.843, p-value = 0.000*) with SWC_{TDR} compared to K_{r250} (*r = 0.802, p-value = 0.000*) (Fig. 5). According to previous studies, EC_a generally covaries with SWC (Altdorff et al., 2017; Calamita et al., 2015; Toy et al., 2010). In this study, VCP_1 and HCP_1 also showed strong positive correlations with SWC_{TDR}. The HCP_1 showed a higher correlation (*r = 0.878, p-value = 0.000*) with SWC_{TDR} compared to VCP_1 (*r = 0.797, p-value = 0.000*) (Fig. 6), and both correlations are statistically significant (*p-value < 0.05*).

3.3. Principal component analysis

The PCA biplot effectively illustrates and explains the data using two principal components (PC1 and PC2), which together explain 87.27 % of the variance. Data points from the same stage (BKG and EOI) are grouped closely together, indicating their similar principal component scores, while the different stages; BKG and EOI exhibit a distinct separation (Fig. 7). In particular, BKG is characterized by relatively lower PCA scores, while EOI displays relatively higher PCA scores along the PC1(Fig. 7). All these tested variables (SWC_{TDR}, SWC_{250}, SWC_{500}, HCP_1, and VCP_1) projected in the same direction as PC1, indicating a positive correlation with PC1 (Fig. 7). Furthermore, these variables exhibit closer proximity to each other and a strong positive correlation (Fig. 7), thus justifying their selection for the development of regression models.

Table 2
Results of one-way analysis of variance (ANOVA) and Tukey tests of time domain reflectometry (TDR) measured soil water contents (SWC) and proxies of ground-penetrating radar (GPR) and electromagnetic induction (EMI) before irrigation (BKG) and after end of irrigation (EOI).

Data set	n	Mean-BKG	Mean-EOI	F-value	p-value
SWC_{TDR} (cm/m)	30	9.35^a	18.18^b	30.06	0.000
K_{r500}	30	5.15^a	9.19^b	55.79	0.000
K_{r250}	30	5.14^a	6.83^b	14.93	0.001
VCP_1 (mS/m)	30	0.96^a	1.44^b	8.06	0.008
HCP_1 (mS/m)	30	1.23^a	2.89^b	295.83	0.000

n – number of samples, p-value – probability value.
The mean difference is significant at the 0.05 level: $F_{crit.} = 4.196$.
The letters (a, b) indicate significant differences between each stage of BKG, and EOI based on the Tukey's test.

3.4. Volumetric soil water content estimated from GPR and TDR

The scatter plots and the regressions between SWC_{TDR} and SWC_{GPR} in both 500 MHz (SWC_{500}; $R^2 = 0.95$) and 250 MHz (SWC_{250}; $R^2 = 0.93$) revealed high accuracy, implying that GPR provides a valid estimation of SWC (Fig. 8). A higher accuracy and better agreement with the 1:1 line of SWC_{500} could be due to a comparable sampling depth of a 500 MHz antenna with SWC_{TDR} than that of a 250 MHz antenna (Fig. 8). Calculated sampling depth for GPR 500 MHz (0–0.19 ± 0.03 m) is relatively similar to the TDR sampling depth (0–0.20 m). On the other hand, the sampling depth calculated for GPR 250 MHz (0–0.35 ± 0.04 m) is relatively higher than the TDR sampling depth. SWC_{TDR} and SWC_{GPR} are close to each other at low water contents. With the applied irrigation, the upper soil layer (0–0.2 m) becomes wetter than the deeper layers (<0.2 m is wet and >0.2 m is dry because the applied water amount is not enough to wet the deep soil layers). The instruments record an average value (bulk soil K_r). Since the deeper layer is relatively dry and due to averaging over the sampling depth, 250 MHz GPR gives under estimations compared to TDR and 500 MHz GPR (TDR and 500 MHz sampling depths are wet, in 250 MHz, the top half is wet while the rest is dry) (Fig. 8). These results showed that GPR-estimated SWCs are accurate and can be used to calibrate EMI.

3.5. Development of simple linear regression models

Based on the results of one-way ANOVA, correlation, and PCA analyses, VCP_1 and HCP_1 measured EC_a data were selected to develop simple linear regression (SLR) models with SWC_{500} and SWC_{250}. SLR models and their details are shown in Table 3 and Fig. 9. In general, SLR models developed between SWC_{500} and EC_a showed higher R^2 than that of SWC_{250} (Table 3). Specifically, SWC_{500} showed higher R^2 with EC_a responses from shallow depths (VCP_1 and HCP_1) than the SWC_{250}.

The intercept of the SLR model represents the EC of the subsurface when SWC is zero. According to the developed SLR models, intercept values were reported as very low (<0.32 mS/m). The EC of dry sand is zero in principle since sand is resistive, whereas Annan, (2005) reported it to be around 0.01 mS/m. The texture of the studied site contains higher sand percentage (sand content > 80 %). Therefore, the studied site's slightly higher intercept values (0.01 < intercept > 0.4 mS/m) could be acceptable as it contains silt and clay, and the soil is not completely dry.

3.6. Evaluation of simple linear regression models

Evaluation of developed SLR models revealed that the prediction accuracy of the developed model is low and deviated from the 1:1 line. VCP_1 predicted SWCs were underestimated, while HCP_1 predicted SWCs were overestimated compared to the GPR estimated SWC in both 500 MHz and 250 MHz (Fig. 10). Variability is high in SWC_{250} compared to SWCs predicted from EMI using developed SLR models from 250 MHz; $VCP_{1,250}$, and $HCP_{1,250}$ (Figs. 10 and 11). Box and whisker plots also clearly show that VCP_1 predicted SWCs ($VCP_{1,500}$, and $VCP_{1,250}$) underestimated and HCP_1 predicted SWCs ($HCP_{1,500}$, $HCP_{1,250}$) overestimated with the SWC_{500} and SWC_{250} (Fig. 11). Additionally, the RMSE of the GPR estimated vs. EMI predicted SWC is less than 5 cm/m in VCP_1 and HCP_1 predicted SWCs with both SWC_{500} and SWC_{250} (Fig. 10). Lin's concordance correlation coefficient showed a poor agreement between GPR-estimated SWC and EMI-predicted SWC for all the developed SLR models (Fig. 10).

Moreover, descriptive statistics in Table 4 reveal that the calibration and evaluation datasets exhibit different ranges. The discrepancy may be attributed to the higher spatial variability observed in the evaluation area, as evidenced by the higher number of samples (n = 260) in the evaluation data set (Table 4 and Appendix Fig. A.2). The evaluation area has a higher SOM variability and lower bulk density compared to the calibration area. In addition, SOM content is higher in shallow depths

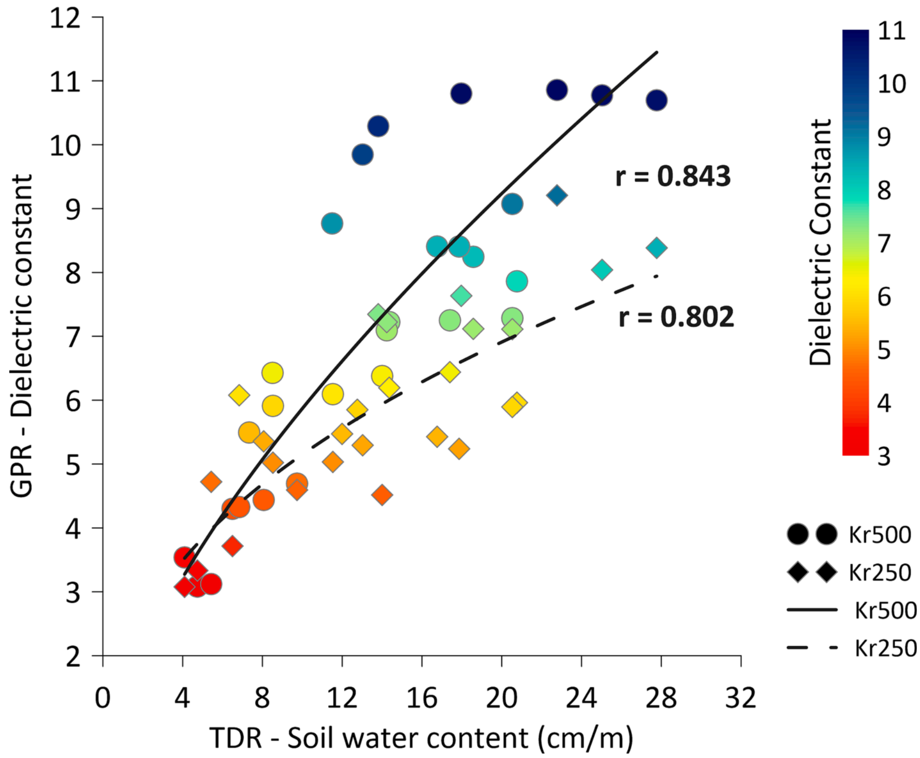

Fig. 5. Scatter plots and correlation coefficients (r) of soil water contents measured from time domain reflectometry (SWC_{TDR}) and dielectric constant of 500 MHz (K_{r500}) and 250 MHz (K_{r250}) transducers.

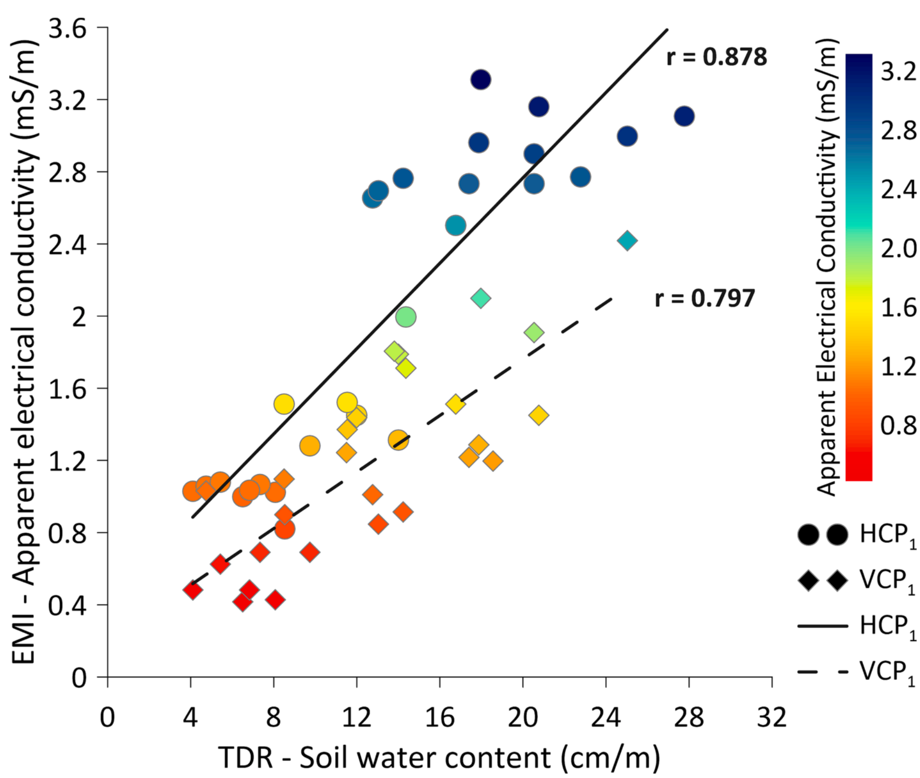

Fig. 6. Scatter plots and correlation coefficients (r) of soil water contents measured from time domain reflectometry (SWC_{TDR}) and apparent electrical conductivity of coil 1 vertical coplanar (VCP_1) and horizontal coplanar (HCP_1).

(thatch layer), while deeper depths consists of increasing amount of sand and gravel. Consequently, the estimated SWC_{500} exceeds SWC_{250} (500 MHz representing shallow depths and 250 MHz for deeper depth), as shallow depths possess greater water-holding capacity than deeper depths under natural conditions in the studied site.

If the EC_a, $SWC_{TDR,}$ and SWC_{GPR} have a higher correlation, these

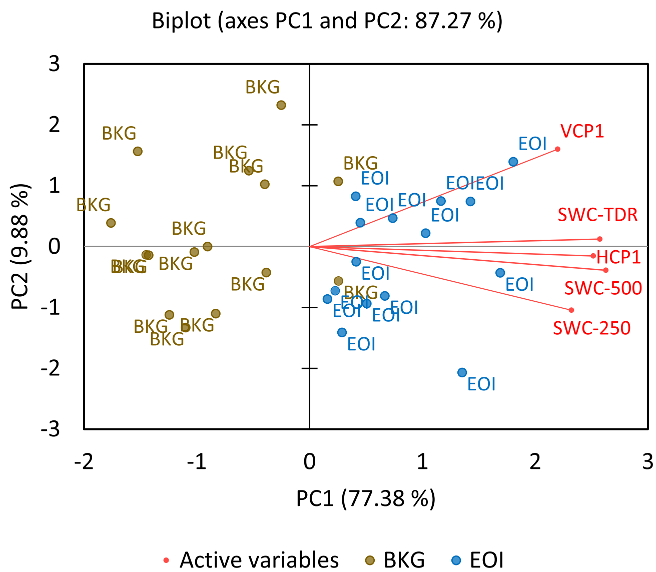

Fig. 7. Principal component analysis (PCA) biplot of ground-penetrating radar estimated soil water contents (SWC_{250} and SWC_{500}), time domain reflectometry measured soil water content (SWC_{TDR}) and electromagnetic induction coil 1 measured apparent electrical conductivities (VCP_1 and HCP_1) under background (BKG) and end of irrigation (EOI).

variables group together (with small angle between variables) in the PCA, and thus SLR results in a higher R^2. EC_a predicted SWCs did not correlate well with GPR estimated SWCs (*i.e.,* deviate from 1:1 line and prediction accuracy is not acceptable). The main reason could be that the EC_a depends not only on the SWC but also on other parameters such as soil temperature, porosity/bulk density, soil texture, and pore-water electrical conductivity (EC_w) (Altdorff et al., 2017; Friedman, 2005; Martini et al., 2017b). For the calibration and evaluation data, temperature corrections were applied; hence, the temperature is assumed to have a minimal or no effect on the developed SLR and model evaluation. In addition, there were no cultivation activities such as tillage during the data collection period; thus, porosity and bulk density could be assumed to be stable. Hence, SWC–EC_a relationship could have been influenced more by the soil texture and pore-water conductivity in the studied site.

According to the literature, EC_w has a more considerable influence on EC_a under irrigated conditions and in low EC soils (Altdorff et al., 2017). In calibration and evaluation data sets, the measured EC_a values in our study ranged from 0 to 4 mS/m, showing relatively low values and variability. Furthermore, it is worth noting that not only in the present study but also in previous research conducted at the same site with multi-coil and multi-frequency EMI instruments it has been consistently showed that EC_a values and their variability are relatively low (Altdorff et al., 2018, 2020; Badewa et al., 2018, 2019). Altdorff et al. (2017) reported EC_a values below 6 mS/m, except for the wet days, whereas Robinet et al. (2018) and Turkeltaub et al. (2022) reported 0–15 and 0–20 mS/m, respectively. In other studies, Robinson et al. (2012) reported values up to 60 mS/m, while Abdu et al. (2008) measured the spatial variation of EC_a ranging from 5 to 120 mS/m. Calamita et al. (2015) reported higher EC_a values and higher variability ranging from 0 to 150 mS/m and André et al. (2012) observed values reaching as high as 200 mS/m in a vineyard with high clay content soils. According to Martini et al. (2017b), in low clay content soils, EC_w has a higher influence on EC_a than SWC, and EC_w could be changed with SWC (Corwin and Lesch, 2003, 2005). In the studied site, the clay content was low (2.4 %), and the sand content was high (82 %). In light of these observations and considering the literature indicating the considerable influence of EC_w on EC_a, especially in low EC soil (Martini et al., 2017b; Corwin and Lesch, 2003, 2005), our findings suggest a nuanced understanding of ECa-SWC relationship in such soil conditions.

In our study, the extremely low EC_a values and their limited range pose challenges for quantitative analysis and calibration in EMI settings. The reduced variability in EC_a led to data points clustering in regression models, resulting in weaker correlations, an issue exacerbated by the low EC_a values due to the reduced signal-to-noise ratio (Altdorff et al., 2017). Our research did not explore the inversion of EC_a data due to the requirement of high-quality data for all coil spacings and orientations.

Table 3
Slope, intercept, and coefficient of determination (R^2) of the developed simple linear regression models.

	Slope	Intercept	R^2
SWC_{500} and VCP_1	0.0915	0.0494	0.71
SWC_{500} and HCP_1	0.1382	0.3138	0.80
SWC_{250} and VCP_1	0.1220	−0.0860	0.47
SWC_{250} and HCP_1	0.1998	0.0759	0.51

All 4 SLR models are statistically significant, p-value < 0.05)

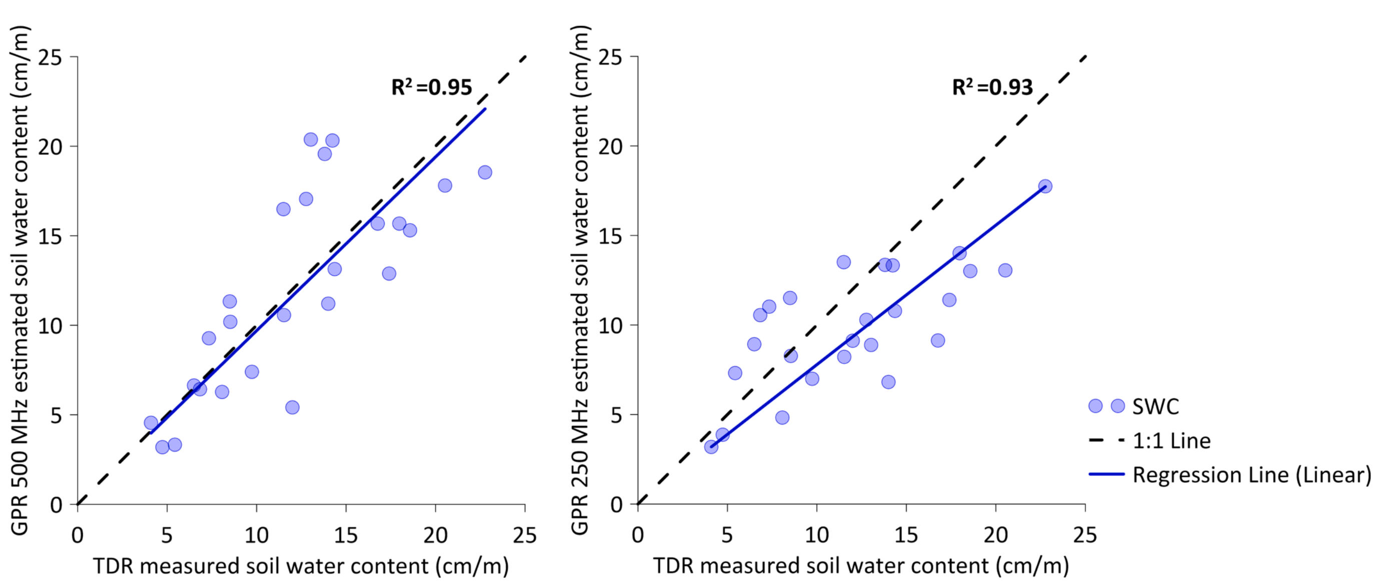

Fig. 8. Scatter plots of soil water content (SWC) measured from time domain reflectometry (SWC_{TDR}) versus ground-penetrating radar (SWC_{GPR}) for 500 MHz (left), and 250 MHz (right). The solid lines correspond to the 1:1 line and the dashed lines correspond to the regression line (linear).

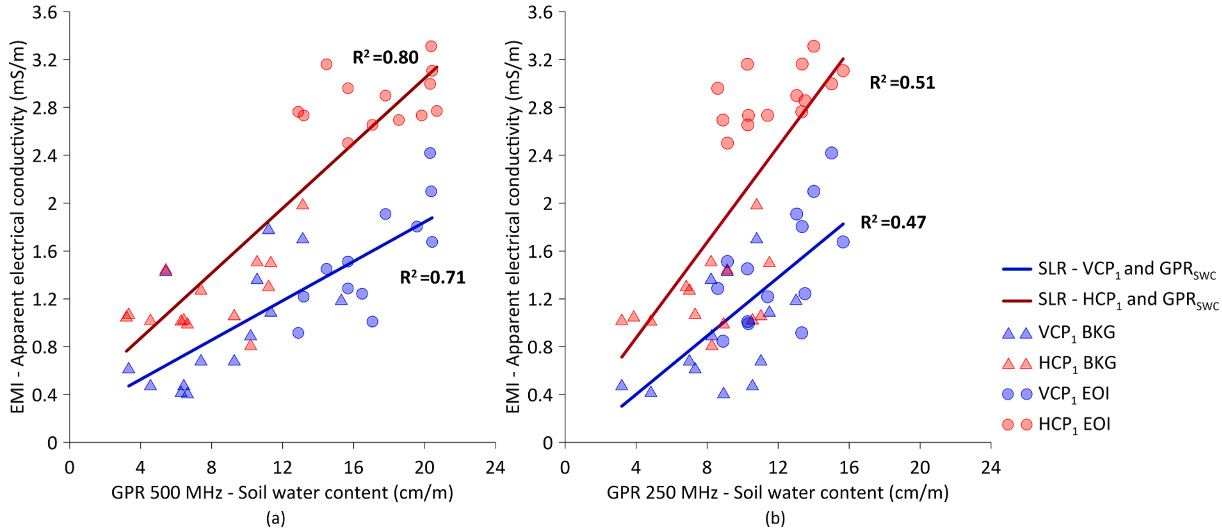

Fig. 9. Soil water contents (SWC) from ground-penetrating radar (GPR); (a) 500 MHz and (b) 250 MHz and the apparent electrical conductivity (EC_a) measured with shallow inter-coil spacing (coil 1) with different coil orientations (VCP_1 and HCP_1) from electromagnetic induction (EMI). Solid lines correspond to the linear regression lines for each data set.

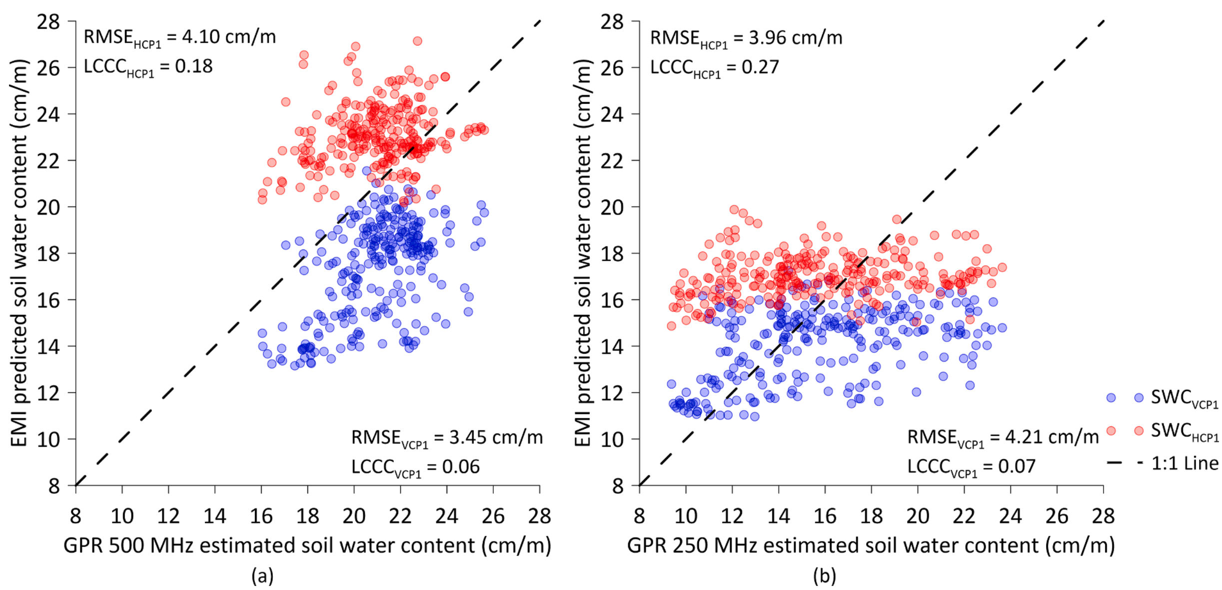

Fig. 10. Scatter plots of ground-penetrating radar (GPR) a) 500 MHz and b) 250 MHz estimated soil water contents (SWCs) versus electromagnetic induction (EMI) predicted SWCs. The dash lines correspond to the 1:1 line.

Furthermore, considerations of soil layering with TDR and GPR were not included, aligning with our focus on shallow depths under the assumption of soil homogeneity.

Building upon the established context, the controlled conditions of our study, akin to a laboratory experiment on boreal podzolic soil, limit the broader applicability of our findings. Future research should aim to investigate areas with more variable EC_a and SWC conditions, including higher EC_a values. It is essential to develop methodologies applicable to different soil textures, scales, and climates. This expansion is necessary for developing robust regression models suitable for heterogeneous conditions. While our study faces limitations due to the low EC_a values and their limited range, it lays the groundwork for more comprehensive future investigations. We propose extending the research to cover a broader spectrum of conditions and employing in-depth data processing techniques, including calibration, conversion, and inversion of EC_a data, (von Hebel et al., 2019) to enhance the applicability of our novel approach in varied soil environments.

In contrast, under saline conditions, EMI responses mainly reflect the soil's electrical conductivity rather than SWC. On the other hand, GPR signals are strongly attenuated under high saline conditions. Therefore, further studies should concentrate on the limitations and applicability of these prediction models under high saline conditions. In addition, GPR is also an indirect method for SWC estimation using K_r, and therefore precise time picking and thorough data processing is essential when employed to calibrate EMI. This study was conducted with default antenna offset for 500 MHz and 250 MHz antennas (Table 2). Future investigations should explore different antenna offsets to find out the best configuration, align with EMI footprint consideration and accurate time picking especially in dry conditions, to distinguish direct ground wave travel time and direct air wave travel time. Small-scale errors might be acceptable for large-scale applications even though improving prediction accuracy in future research will necessitate efforts to minimize these limitations inherent to indirect geophysical methods.

On the other hand, GPR estimated SWC almost only depends on

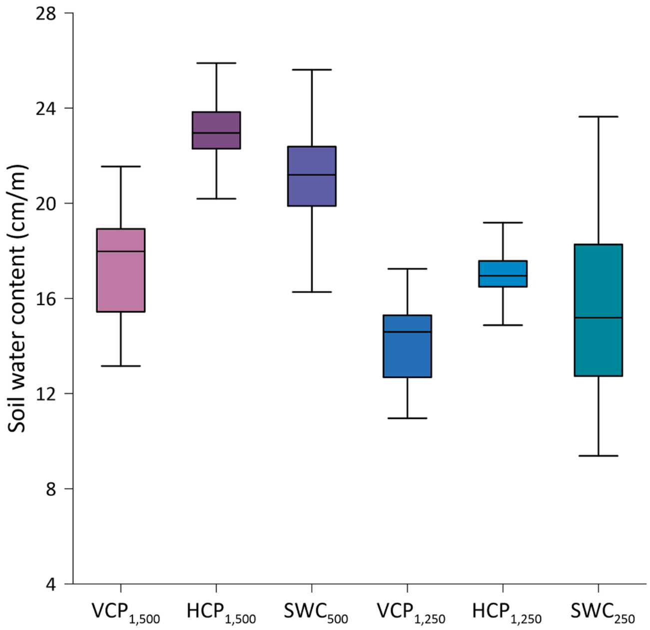

Fig. 11. Comparison of soil water content (SWC) variability predicted from electromagnetic induction (EMI) using developed regression models and estimated from 250 MHz (SWC_{250}) and 500 MHz (SWC_{500}) ground-penetrating radar (GPR).

relative permittivity (K_r). Responses of GPR, *i.e.*, direct ground wave travel time and, therefore, the velocity (V_{DGW}), change with changing SWC (Annan, 2005). Though EMI measured EC_a depends on several other parameters as mentioned above, EC_a predicted SWC does not reflect only the SWC (change of EC_a could not only be due to change of SWC). Therefore, all the interrelated factors must be considered when estimating SWC, especially in low EC_a and sandy-rich sites using EMI. Under natural conditions in a highly heterogeneous medium like soil, all the properties are interrelated, and model prediction accuracy and precision can be achieved by considering the combined effect of soil properties. Furthermore, GPR performs effectively in soils that are rich in sand, in contrast to EMI methods. In order to accurately predict not only SWC but also other important soil properties using EC_a, it is necessary to transition from SLR models to multiple linear regression models by considering different existing models such as Archie's law and Rhoade's equation (Archie, 1942; Rhoades et al., 1976).

The representation of the sampling volume in the soil differs among GPR, EMI and TDR. The GPR and EMI approximated as half of an ellipsoid and TDR as a cylinder as documented previously (Galagedara et al., 2003b; Limsuwat et al., 2008). TDR exhibits a constant sensitivity over depth, whereas GPR and VCP sensitivity decreases as depth increases (Appendix Fig. A.1). However, HCP sensitivity behaves differently, initially increasing and then decreasing (Appendix Fig. A.1). Based on the calculations, Table 5 shows the considered sampling volumes of each sensor. GPR (at both frequencies) covers a larger sampling volume than the TDR (Table 5). Therefore, GPR offers the potential to cover a broader range of EMI's footprint and sampling volume compared to TDR.

4. Conclusion

In this study, we used dielectric constant (K_r) and apparent electrical conductivity (EC_a) as proxies of ground-penetrating radar (GPR) and electromagnetic induction (EMI), respectively, in order to develop and assess regression models for soil water content (SWC) estimation. Two GPR frequencies, specifically 250 MHz and 500 MHz, along with two EMI coil orientations, vertical coplanar (VCP) and horizontal coplanar (HCP), with 0.32 m inter coil spacing, were correlated with each other and with SWC measured using time domain reflectometry (SWC_{TDR}). Among these variables, K_{r250}, K_{r500}, VCP_1, and HCP_1 displayed strong positive correlations with SWC_{TDR}. In order to meet the desired sampling depth range, we excluded coils 2 and 3 data from the regression model development for this study. The estimated SWC from GPR (SWC_{250} and SWC_{500}) exhibited satisfactory accuracy with high R^2 values (>0.90), indicating their potential suitability for calibrating EMI to estimate SWC. Simple linear regression (SLR) models constructed between VCP_1 and HCP_1 with SWC_{500} demonstrated higher R^2 values than those obtained with SWC_{250}. Nevertheless, during the evaluation phase, the SLR models were not successful as expected to predict SWCs from EMI using the estimated SWC_{GPR}.

This study introduces a novel approach, the first of its kind, highlighting the potential of GPR in calibrating EMI for SWC estimation. Both methods offer similar sampling volumes compared to point-scale time domain reflectometry (TDR) measurements, which are impractical and time-consuming when covering the large sampling areas required for EMI. The findings suggest that GPR can be a valuable tool for EMI calibration and SWC estimation. Nonetheless, further research is required to elucidate the effect of varying SWC conditions, including variations in soil textures (clay-rich soils), high EC_a soils, and landscapes characterized by higher EC_a and SWC variability. This will contribute to our understating of the EMI–GPR relationship and to improve the calibration and evaluation process.

The subsurface exhibits a complex interplay of various soil properties and conditions alongside SWC in natural environments. Therefore, in precision agriculture, where the identification of management zones for irrigation and other agricultural practices is crucial, it is imperative to consider this combined effect to obtain vital decision-making information. Future research endeavors should focus on enhancing the EMI technique to evaluate how this combined effect influences the EC_a and enables the prediction of SWC and other significant soil properties and

Table 5
Approximate sampling depths and volumes of time domain reflectometry (TDR), ground-penetrating radar (GPR), and electromagnetic induction (EMI).

Sensor	Sampling depth (m)	Approximate sampling volume (cm^3)
TDR	0–0.20	90
GPR 500 MHz	0–0.19*	17,396
GPR 250 MHz	0–0.35*	97,533
EMI VCP_1	0–0.25*	41,904
EMI HCP_1	0–0.50*	167,619

* Approximate values.

Table 4
Descriptive statistics of studied variables in the calibration and evaluation data set.

Variable	Calibration data set (n = 30)				Evaluation data set (n = 260)			
	Min	Max	Mean	Standard deviation	Min	Max	Mean	Standard deviation
SWC_{500} (cm/m)	3.2	20.7	12.9	5.7	16.0	25.6	21.0	1.9
SWC_{250} (cm/m)	3.2	17.7	10.3	3.4	9.4	23.6	15.7	3.7
VCP_1 (mS/m)	0.4	2.4	1.2	0.5	1.3	2.0	1.6	0.2
HCP_1 (mS/m)	0.8	3.3	2.1	0.9	3.0	4.0	3.5	0.2
SWC_{TDR} (cm/m)	4.1	27.8	13.8	6.2	–	–	–	–

conditions. This can be achieved by integrating different geophysical or standard methods, thereby expanding the applications of EMI in estimating the spatial and temporal variations of soil properties and conditions within the agricultural landscape. Such advancements would greatly support the implementation of precision agriculture.

Funding

This research was funded by Natural Sciences and Engineering Research Council of Canada, Discovery Grant (NSERC-DG): RGPIN-2019-04614, Industry, Energy and Innovation (IET) of the Government of Newfoundland and Labrador, Grant: 5404-1962-102, and Grenfell Campus, Memorial University of Newfoundland.

CRediT authorship contribution statement

Sashini Pathirana: Conceptualization, Data curation, Formal analysis, Investigation, Methodology, Visualization, Writing – original draft. **Sébastien Lambot:** Methodology, Supervision, Validation, Writing – review & editing. **Manokararajah Krishnapillai:** Validation, Writing – review & editing. **Christina Smeaton:** Supervision, Validation, Writing – review & editing. **Mumtaz Cheema:** Validation, Writing – review & editing. **Lakshman Galagedara:** Conceptualization, Funding acquisition, Investigation, Methodology, Project administration, Resources, Supervision, Validation, Writing – review & editing.

Declaration of competing interest

The authors declare the following financial interests/personal relationships which may be considered as potential competing interests: 'Lakshman Galagedara reports financial support was provided by Natural Sciences and Engineering Research Council of Canada. Lakshman Galagedara reports financial support was provided by Industry, Energy and Innovation (IET) of the Government of Newfoundland and Labrador'.

Data availability

Data will be made available on request.

Acknowledgement

The authors would like to express sincere gratitude to the independent reviewers for their valuable time and constructive feedback, which significantly improved the quality of this paper.

The authors extend special appreciation to Adrian Reid and the other staff members of the Department of Fisheries, Forestry, and Agriculture, Government of Newfoundland and Labrador, for their provision and oversight of the research field.

Appendix A. Supplementary material

Supplementary material to this article can be found online at https://doi.org/10.1016/j.jhydrol.2024.130957.

References

Abdu, H., Robinson, D.A., Seyfried, M., Jones, S.B., 2008. Geophysical imaging of watershed subsurface patterns and prediction of soil texture and water holding capacity. Water Resour. Res. 44 (4) https://doi.org/10.1029/2008WR007043.

Altdorff, D., von Hebel, C., Borchard, N., van der Kruk, J., Bogena, H.R., Vereecken, H., Huisman, J.A., 2017. Potential of catchment-wide soil water content prediction using electromagnetic induction in a forest ecosystem. Environ. Earth Sci. 76 (3), 111. https://doi.org/10.1007/s12665-016-6361-3.

Altdorff, D., Galagedara, L., Nadeem, M., Cheema, M., Unc, A., 2018. Effect of agronomic treatments on the accuracy of soil moisture mapping by electromagnetic induction. Catena 164, 96–106. https://doi.org/10.1016/j.catena.2017.12.036.

Altdorff, D., Sadatcharam, K., Unc, A., Krishnapillai, M., Galagedara, L., 2020. Comparison of multi-frequency and multi-coil electromagnetic induction (EMI) for mapping properties in shallow podsolic soils. Sensors 20 (8), Article 8. https://doi.org/10.3390/s20082330.

André, F., Van Leeuwen, C., Saussez, S., Van Durmen, R., Bogaert, P., Moghadas, D., De Rességuier, L., Delvaux, B., Vereecken, H., Lambot, S., 2012. High-resolution imaging of a vineyard in south of France using ground-penetrating radar, electromagnetic induction and electrical resistivity tomography. J. Appl. Geophys. 78, 113–122. https://doi.org/10.1016/j.jappgeo.2011.08.002.

Annan, A.P., 2005. Ground-Penetrating Radar. In: Butler, D.K. (Ed.), Near-Surface Geophysics (vol. 13, p. 0). Society of Exploration Geophysicists. https://doi.org/10.1190/1.9781560801719.ch11.

Archie, G.E., 1942. The electrical resistivity log as an aid in determining some reservoir characteristics. Trans. AIME 146, 54–62. https://doi.org/10.2118/942054-G.

Badewa, E., Unc, A., Cheema, M., Kavanagh, V., Galagedara, L., 2018. Soil moisture mapping using multi-frequency and multi-coil electromagnetic induction sensors on managed podzols. Agronomy 8 (10), 224. https://doi.org/10.3390/agronomy8100224.

Badewa, E., Unc, A., Cheema, M., Galagedara, L., 2019. Temporal stability of soil apparent electrical conductivity (ECa) in managed podzols. Acta Geophys. 67 (4), 1107–1118. https://doi.org/10.1007/s11600-019-00306-1.

Binley, A., Hubbard, S.S., Huisman, J.A., Revil, A., Robinson, D.A., Singha, K., Slater, L. D., 2015. The emergence of hydrogeophysics for improved understanding of subsurface processes over multiple scales. Water Resour. Res. 51 (6), 3837–3866. https://doi.org/10.1002/2015WR017016.

Brevik, E.C., Fenton, T.E., Lazari, A., 2006. Soil electrical conductivity as a function of soil water content and implications for soil mapping. Precis. Agric. 7 (6), 393–404. https://doi.org/10.1007/s11119-006-9021-x.

Calamita, G., Perrone, A., Brocca, L., Onorati, B., Manfreda, S., 2015. Field test of a multi-frequency electromagnetic induction sensor for soil moisture monitoring in southern Italy test sites. J. Hydrol. 529 (1), 316–329. https://doi.org/10.1016/j.jhydrol.2015.07.023.

Chanzy, A., Tarussov, A., Bonn, F., Judge, A., 1996. Soil water content determination using a digital ground-penetrating radar. Soil Sci. Soc. Am. J. 60 (5), 1318–1326. https://doi.org/10.2136/sssaj1996.03615995006000050005x.

Corwin, D.L., Lesch, S.M., 2003. Application of soil electrical conductivity to precision agriculture: Theory, principles, and guidelines. Agron. J. 95 (3), 455–471. https://doi.org/10.2134/agronj2003.4550.

Corwin, D.L., Lesch, S.M., 2005. Apparent soil electrical conductivity measurements in agriculture. Comput. Electron. Agric. 46 (1–3), 11–43. https://doi.org/10.1016/j.compag.2004.10.005.

Davis, J.L., Annan, A.P., 1989. Ground-penetrating radar for high-resolution mapping of soil and rock stratigraphy. Geophys. Prospect. 37 (5), 531–551. https://doi.org/10.1111/j.1365-2478.1989.tb02221.x.

Doolittle, J.A., Brevik, E.C., 2014. The use of electromagnetic induction techniques in soils studies. Geoderma 223–225, 33–45. https://doi.org/10.1016/j.geoderma.2014.01.027.

Evett, S.R., Parkin, G.W., 2005. Advances in soil water content sensing: The continuing maturation of technology and theory. Vadose Zone J. 4 (4), 986–991. https://doi.org/10.2136/vzj2005.0099.

Ferré, P.A., Rudolph, D.L., Kachanoski, R.G., 1996. Spatial averaging of water content by time domain reflectometry: Implications for twin rod probes with and without dielectric coatings. Water Resour. Res. 32 (2), 271–279. https://doi.org/10.1029/95WR02576.

Friedman, S.P., 2005. Soil properties influencing apparent electrical conductivity: A review. Comput. Electron. Agric. 46 (1–3), 45–70. https://doi.org/10.1016/j.compag.2004.11.001.

Galagedara, L.W., Parkin, G.W., Redman, J.D., 2003a. An analysis of the ground-penetrating radar direct ground wave method for soil water content measurement. Hydrol. Process. 17 (18), 3615–3628. https://doi.org/10.1002/hyp.1351.

Galagedara, L.W., Parkin, G.W., Redman, J.D., Endres, A.L., 2003b. Assessment of soil moisture content measured by borehole GPR and TDR under transient irrigation and drainage. J. Environ. Eng. Geophys. 8 (2), 77–86. https://doi.org/10.4133/JEEG8.2.77.

Galagedara, L.W., Redman, J.D., Parkin, G.W., Annan, A.P., Endres, A.L., 2005. Numerical modeling of GPR to determine the direct ground wave sampling depth. Vadose Zone J. 4 (4), 1096–1106. https://doi.org/10.2136/vzj2004.0143.

Grote, K., Anger, C., Kelly, B., Hubbard, S., Rubin, Y., 2010. Characterization of soil water content variability and soil texture using GPR groundwave techniques. J. Environ. Eng. Geophys. 15 (3), 93–110. https://doi.org/10.2113/JEEG15.3.93.

Huisman, J.A., Sperl, C., Bouten, W., Verstraten, J.M., 2001. Soil water content measurements at different scales: Accuracy of time domain reflectometry and ground-penetrating radar. J. Hydrol. 245 (1), 48–58. https://doi.org/10.1016/S0022-1694(01)00336-5.

Huisman, J.A., Hubbard, S.S., Redman, J.D., Annan, A.P., 2003. Measuring soil water content with ground penetrating radar: A review. Vadose Zone J. 2 (4), 476–491. https://doi.org/10.2113/2.4.476.

Jones, S.B., Wraith, J.M., Or, D., 2002. Time domain reflectometry measurement principles and applications. Hydrol. Process. 16 (1), 141–153. https://doi.org/10.1002/hyp.513.

Kachanoski, R., Gregorich, E., Van Wesenbeeck, I., 1998. Estimating spatial variations of soil water content using noncontacting electromagnetic inductive methods. Can. J. Soil Sci. 68, 715–722. https://doi.org/10.4141/cjss88-069.

Klotzsche, A., Jonard, F., Looms, M.C., van der Kruk, J., Huisman, J.A., 2018. Measuring soil water content with ground penetrating radar: A decade of progress. Vadose Zone J. 17 (1), 1–9. https://doi.org/10.2136/vzj2018.03.0052.

Limsuwat, A., Sakaki, T., Illangasekare, T.H., 2008. Experimental quantification of bulk sampling volume of ECH₂O soil moisture sensors. https://doi.org/10.25675/10217/200717.

Liu, X., Chen, J., Cui, X., Liu, Q., Cao, X., Chen, X., 2019. Measurement of soil water content using ground-penetrating radar: A review of current methods. Int. J. Digital Earth 12 (1), 95–118. https://doi.org/10.1080/17538947.2017.1412520.

Mahmoudzadeh Ardekani, M.R., 2013. Off- and on-ground GPR techniques for field-scale soil moisture mapping. Geoderma 200–201, 55–66. https://doi.org/10.1016/j.geoderma.2013.02.010.

Martini, E., Werban, U., Zacharias, S., Pohle, M., Dietrich, P., Wollschläger, U., 2017a. Repeated electromagnetic induction measurements for mapping soil moisture at the field scale: Validation with data from a wireless soil moisture monitoring network. Hydrol. Earth Syst. Sci. 21 (1), 495–513. https://doi.org/10.5194/hess-21-495-2017.

Martini, E., Wollschläger, U., Musolff, A., Werban, U., Zacharias, S., 2017b. Principal component analysis of the spatiotemporal pattern of soil moisture and apparent electrical conductivity. Vadose Zone J. 16 (10) https://doi.org/10.2136/vzj2016.12.0129.

McNeill, J.D., 1980. Electromagnetic Terrain Conductivity Measurement at Low Induction Numbers. Geonics. Ltd., Technical Note TN-6, Mississauga, Canada.

Mensah, C., Katanda, Y., Krishnapillai, M., Cheema, M., Galagedara, L., 2023a. Estimation of soil water content using electromagnetic induction sensors under different land uses. Environ. Res. Commun. 5 (8), 1–22. https://doi.org/10.1088/2515-7620/acebbd.

Mensah, C., Katanda, Y., Krishnapillai, M., Cheema, M., Galagedara, L., 2023b. Multi-frequency electromagnetic induction soil moisture characterization under different land uses in western Newfoundland. Can. J. Soil Sci. 103 (3), 446–461. https://doi.org/10.1139/CJSS-2022-0102.

Minet, J., Bogaert, P., Vanclooster, M., Lambot, S., 2012. Validation of ground penetrating aradar full-waveform inversion for field scale soil moisture mapping. J. Hydrol. 424–425, 112–123. https://doi.org/10.1016/j.jhydrol.2011.12.034.

Pathirana, S., Lambot, S., Krishnapillai, M., Cheema, M., Smeaton, C., Galagedara, L., 2023. Ground-penetrating radar and electromagnetic induction: Challenges and opportunities in agriculture. Remote Sens. (Basel) 15 (11), 2932. https://doi.org/10.3390/rs15112932.

Rhoades, J.D., Raats, P.A.C., Prather, R.J., 1976. Effects of liquid-phase electrical conductivity, water content, and surface conductivity on bulk soil electrical conductivity. Soil Sci. Soc. Ammerica J. 40, 651–655. https://doi.org/10.2136/sssaj1976.03615995004000050017x.

Robinet, J., von Hebel, C., Govers, G., van der Kruk, J., Minella, J.P.G., Schlesner, A., Ameijeiras-Mariño, Y., Vanderborght, J., 2018. Spatial variability of soil water content and soil electrical conductivity across scales derived from electromagnetic induction and time domain reflectometry. Geoderma 314, 160–174. https://doi.org/10.1016/j.geoderma.2017.10.045.

Robinson, D.A., Campbell, C.S., Hopmans, J.W., Hornbuckle, B.K., Jones, S.B., Knight, R., Ogden, F., Selker, J., Wendroth, O., 2008. Soil moisture measurement for ecological and hydrological watershed-scale observatories: A review. Vadose Zone J. 7 (1), 358–389. https://doi.org/10.2136/vzj2007.0143.

Robinson, D.A., Abdu, H., Lebron, I., Jones, S.B., 2012. Imaging of hill-slope soil moisture wetting patterns in a semi-arid oak savanna catchment using time-lapse electromagnetic induction. J. Hydrol. 416–417, 39–49. https://doi.org/10.1016/j.jhydrol.2011.11.034.

Rubin, Y., Hubbard, S.S. (Eds.), 2005. Hydrogeophysics. Springer.

Sheets, K.R., Hendrickx, J.M.H., 1995. Noninvasive soil water content measurement using electromagnetic induction. Water Resour. Res. 31 (10), 2401–2409. https://doi.org/10.1029/95WR01949.

Soil Classification Working Group, 1998. The Canadian System of Soil Classification, 3rd ed. Agriculture and Agri-Food Canada Publication, Ottawa.

Steelman, C.M., Endres, A.L., 2011. Comparison of petrophysical relationships for soil moisture estimation using GPR ground waves. Vadose Zone J. 10 (1), 270–285. https://doi.org/10.2136/vzj2010.0040.

Topp, G.C., Davis, J.L., Annan, A.P., 1980. Electromagnetic determination of soil water content: Measurements in coaxial transmission lines. Water Resour. Res. 16 (3), 574–582. https://doi.org/10.1029/WR016i003p00574.

Toy, C.W., Steelman, C.M., Endres, A.L., 2010. Comparing electromagnetic induction and ground penetrating radar techniques for estimating soil moisture content. In: Proceedings of the XIII International Conference on Ground Penetrating Radar, pp. 1–6. https://doi.org/10.1109/ICGPR.2010.5550068.

Turkeltaub, T., Wang, J., Cheng, Q., Jia, X., Zhu, Y., Shao, M., Binley, A., 2022. Soil moisture and electrical conductivity relationships under typical Loess Plateau land covers. Vadose Zone J. 21 (1) https://doi.org/10.1002/vzj2.20174.

Vereecken, H., Huisman, J.A., Bogena, H., Vanderborght, J., Vrugt, J.A., Hopmans, J.W., 2008. On the value of soil moisture measurements in vadose zone hydrology: A review: soil moisture and hydrology. Water Resour. Res. 44 (4) https://doi.org/10.1029/2008WR006829.

Vereecken, H., Huisman, J.A., Pachepsky, Y., Montzka, C., van der Kruk, J., Bogena, H., Weihermüller, L., Herbst, M., Martinez, G., Vanderborght, J., 2014. On the spatio-temporal dynamics of soil moisture at the field scale. J. Hydrol. 516, 76–96. https://doi.org/10.1016/j.jhydrol.2013.11.061.

Vereecken, H., Schnepf, A., Hopmans, J.W., Javaux, M., Or, D., Roose, T., Vanderborght, J., Young, M.H., Amelung, W., Aitkenhead, M., Allison, S.D., Assouline, S., Baveye, P., Berli, M., Brüggemann, N., Finke, P., Flury, M., Gaiser, T., Govers, G., Ghezzehei, T., Hallett, P., Hendricks Franssen, H.J., Heppell, J., Horn, R., Huisman, J.A., Jacques, D., Jonard, F., Kollet, S., Lafolie, F., Lamorski, K., Leitner, D., McBratney, A., Minasny, B., Montzka, C., Nowak, W., Pachepsky, Y., Padarian, J., Romano, N., Roth, K., Rothfuss, Y., Rowe, E.C., Schwen, A., Šimůnek, J., Tiktak, A., Van Dam, J., van der Zee, S.E.A.T.M., Vogel, H.J., Vrugt, J.A., Wöhling, T., Young, I.M., 2016. Modeling soil processes: Review, key challenges, and new perspectives. Vadose Zone J. 15 (5), 1–57. https://doi.org/10.2136/vzj2015.09.0131.

von Hebel, C., van der Kruk, J., Huisman, J.A., Mester, A., Altdorff, D., Endres, A.L., Zimmermann, E., Garré, S., Vereecken, H., 2019. Calibration, Conversion, and 757 Quantitative Multi-Layer Inversion of Multi-Coil Rigid-Boom Electromagnetic Induction 758 Data. Sensors 19 (21), 4753. https://doi.org/10.3390/s19214753.

Weiler, K.W., Steenhuis, T.S., Boll, J., Kung, K.-J., 1998. Comparison of ground penetrating radar and time-domain reflectometry as soil water sensors. Soil Sci. Soc. Am. J. 62 (5), 1237–1239. https://doi.org/10.2136/sssaj1998.03615995006200050013x.

Wijewardana, Y.G.N.S., Galagedara, L.W., 2010. Estimation of spatio-temporal variability of soil water content in agricultural fields with ground penetrating radar. J. Hydrol. 391 (1–2), 24–33. https://doi.org/10.1016/j.jhydrol.2010.06.036.

Wu, K., Rodriguez, G.A., Zajc, M., Jacquemin, E., Clément, M., De Coster, A., Lambot, S., 2019. A new drone-borne GPR for soil moisture mapping. Remote Sens. Environ. 235, 111456 https://doi.org/10.1016/j.rse.2019.111456.

Wu, K., Desesquelles, H., Cockenpot, R., Guyard, L., Cuisiniez, V., Lambot, S., 2022. Ground-penetrating radar full-wave inversion for soil moisture mapping in Trench-hill potato fields for precise irrigation. Remote Sens. (Basel) 14 (23), 6046. https://doi.org/10.3390/rs14236046.

Wu, K., Lambot, S., 2022. Analysis of low-frequency drone-borne GPR for root-zone soil electrical conductivity characterization. IEEE Trans. Geosci. Remote Sens. 60, 1–13. https://doi.org/10.1109/TGRS.2022.3198431.